Chapter 11
Polymer-Derived Ceramics: A Novel Inorganic Thermoelectric Material System

Rakesh Krishnamoorthy Iyer, Adhimoolam Bakthavachalam Kousaalya, and Srikanth Pilla

Abstract Ever-increasing global energy consumption and its resultant impact on climate change have pushed researchers toward the development of multiple novel sustainable technologies. Among these technologies, utilization of waste heat energy via use of thermoelectric generators (TEGs) has gained credence over the past few years, especially given the vast improvement in TEGs conversion efficiency through innovative and unique thermoelectric (TE) materials. However, these improvements have been marked by concerns regarding poor thermal and mechanical stability at higher (operational) temperatures, as well as toxicity and high cost of specific elements used in such TEGs, thereby rendering TEGs unfit for commercial purposes. Polymer-derived ceramics (PDCs) offer a possible solution to this unsolved conundrum, given the excellent mechanical and thermal stability of PDCs (till as high as 2000 °C), along with the relatively low toxicity and abundance of elements used in such systems. PDCs also provide the opportunity for tuning of microstructure to achieve the desired properties via control of polymeric precursor and processing parameters. This chapter provides an overview of PDCs, focusing on TE properties of PDCs in detail, especially with regard to changes in operational temperature, as well as the underlying electrical conduction mechanism observed in these PDCs. Finally, a succinct summary of the existing literature, as well as the desired direction of work for truly harnessing potential as commercial thermoelectrics, has also been provided.

R. K. Iyer · A. B. Kousaalya
Department of Automotive Engineering, Clemson University, Greenville, SC, USA

Clemson Composites Center, Clemson University, Greenville, SC, USA

S. Pilla (✉)
Department of Automotive Engineering, Clemson University, Greenville, SC, USA

Clemson Composites Center, Clemson University, Greenville, SC, USA

Department of Materials Science and Engineering, Clemson University, Clemson, SC, USA

Department of Mechanical Engineering, Clemson University, Clemson, SC, USA
e-mail: spilla@clemson.edu

S. Skipidarov, M. Nikitin (eds.), *Novel Thermoelectric Materials and Device Design Concepts*, https://doi.org/10.1007/978-3-030-12057-3_11

11.1 Introduction

Ever-increasing global energy consumption and its associated impacts on anthropogenic climate change have led to enhanced attention on sustainable, clean, and green energy technologies. Among such technologies, efficient generation and utilization of energy by conversion of waste heat to electricity via TEGs remains an attractive possibility. TEGs can be highly beneficial for sectors and processes that generate enormous amounts of waste heat, such as home heating, nuclear and thermal power plants, automotive exhausts, industrial processes, and waste incineration, all of which together cause wastage of approximately two-thirds of total primary energy used [1]. Application of TEGs across all these sectors can help improve the efficiency of fossil fuel usage, reduce the associated consumer bills, and also reduce both pollutant and greenhouse gas emissions, thereby mitigating local pollution and climate change, as well as resultant impacts on our planet.

However, commercial application of TEGs necessitates high conversion efficiencies (from waste heat to electricity), exceeding 5% [2]. Efficiency (η) of TEG is determined by its TE figure of merit (ZT)—a dimensionless quantity that is desired to be high for a material to exhibit excellent TE performance (Eq. 11.1). ZT of a material in turn is a function of three properties: thermal conductivity (κ) which can be divided into electronic (κ_e) and lattice (κ_L) components, electrical conductivity (σ), and Seebeck coefficient S (Eqs.11.2–11.4). However, achieving high ZT remains a difficult and challenging objective, since electrical and thermal conductivities of any material have a direct correlation through proportionality between σ and κ_e [3].

$$\eta = \frac{T_h - T_c}{T_h} \times \frac{\sqrt{1 + ZT_{avg}} - 1}{\sqrt{1 + ZT_{avg}} + \frac{T_c}{T_h}}, \tag{11.1}$$

where T_h and T_c are temperatures on hot and cold side and ZT_{avg} is average value of TE figure of merit ZT of TE material in temperature gradient between T_c and T_h.

$$ZT = \frac{PF}{\kappa} T, \tag{11.2}$$

$$PF = S^2 \sigma, \tag{11.3}$$

$$\kappa = \kappa_e + \kappa_L, \tag{11.4}$$

where PF, T, κ, S, σ, κ_e, and κ_L are power factor, absolute temperature, total thermal conductivity, Seebeck coefficient, electrical conductivity, electronic thermal conductivity, and lattice thermal conductivity, respectively. Consequently, higher ZT corresponds to higher conversion efficiency.

Despite these limitations, numerous initiatives have been undertaken to reach higher ZT, resulting in the development of several novel TE materials over the past few decades which can be categorized into three groups (Fig. 11.1) [4]. The first

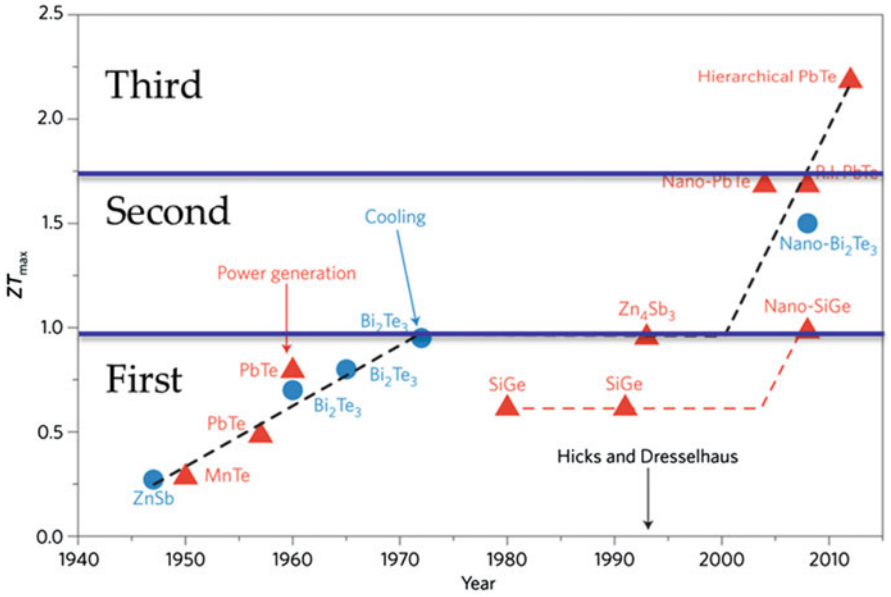

Fig. 11.1 Thermoelectric materials across different generations over the years (reproduced from [4] after modification)

group comprises mainly of four compounds, namely, ZnSb—the first compound that exhibited Seebeck effect [4]—and three naturally occurring semiconductors: Bi_2Te_3, PbTe, and SiGe. While this group achieved a maximum ZT of 1.0, it was believed that all three TE properties (κ, σ, and S) are intrinsic to a TE material and cannot be artificially manipulated. This belief led to a near-complete halt in research in the field of thermoelectrics until the 1990s, when pioneering work by Hicks and Dresselhaus [5, 6] on enhancing ZT via nanostructuring led to a renaissance in this field. This led to the development of second group of thermoelectrics that achieved significant increase in ZT (up to ~1.7) by significantly reducing κ via enhanced phonon scattering. In contrast, the third generation of thermoelectrics, which advent is fairly recent, has focused on the use of initiatives aimed at increase in either/both of σ and S in order to enhance ZT of TE materials beyond 1.8 [7, 8]. Table 11.1 gives a list of prominent TE materials (developed till date) including ZT values.

However, despite the availability of multiple bulk TE materials — both in research and in commercial applications (Table 11.1)—these suffer from a plethora of issues. Most TE materials are highly toxic and brittle and are characterized by poor mechanical properties at temperatures where these materials exhibit the highest ZT value (~0.75 of melting point). Furthermore, most bulk TE materials contain elements with high densities, making those unsuitable for specific uses such as in automobiles, where the focus is on lightweighting vehicles and improving fuel economy [24]. The listed TE materials are also environmentally unsustainable due to the use of highly energy-intensive processing methods for production and often

Table 11.1 Thermoelectric materials: ZT values and other properties

Material	M	T	T_m, °C	H	A	ZT		d, g/cm^3	Ref.
						p-type	*n*-type		
Bi_2Te_3	×	✓	586	×	×	1.9 (320 K)	1.2 (370 K)		[9, 10]
LAST	!	!		×	×	1.7 (800 K)	2.2 (800 K)	8	[11, 12]
PbTe	!	!	924	×	×	2.2 (915 K)	1.6 (775 K)	8.16	[1, 13]
Clathrates	✓	✓		!	×	0.61	1.35 (900 K)	5.8	[14]
$\beta - Zn_4Sb_3$	×	!	567	!	!	1.3 (670 K)	–	6.2	[15]
Skutterudites	!	✓	1350	!	×	0.93	1.7 (850 K)	7.4	[16]
SnSe	×	×	861	×	×	2.6 (900 K)	–	6.18	[17]
Mg_2Si	×	×	1102	✓	✓	0.65	1.3 (700 K)	2	[18]
Half-Heusler	✓	✓		!	!	1 (1073 K)	1 (1073 K)	10	[19]
SiGe	✓	✓		✓	×	1	1.3 (1173 K)	4	[20]
PLEC	!	!		!	✓	1.5 (1000 K)	0.6	6.5	[21]
Zintl phase	!	!		×	×	1.3 (1223 K)	0.86	8.3	[22]
Oxides	!	✓		✓	✓	1.4 (923 K)	1.4 (923 K)	8	[23]

✓ safe, × unsafe, ! OK, M mechanical stability, T thermal stability, H nontoxic, A abundance, T_m melting temperature, d material density

contain rare earth elements that make those very expensive [25]. Further, most TE materials can achieve ZT values only up to ~1.8, while higher conversion efficiency (desired for commercial applications) often necessitates ZT $\geq$ 3 [2].

In light of these issues, this chapter discusses and evaluates the potential of polymer-derived ceramics (PDCs) as an alternative to existing TE materials. The choice of PDCs stems from ability to address the aforementioned issues. PDCs are mainly constituted of low-density elements, are stable up to very high temperatures (~2000 °C), can be processed via energy-efficient methods, and are relatively inexpensive. This chapter presents a succinct introduction of PDCs, followed by a discussion of the existing literature on TE properties of PDCs. Finally, the chapter ends with a section that highlights the probable future direction of research on enhancing thermoelectric potential of PDCs.

11.2 Polymer-Derived Ceramics: A Brief Overview

Polymer-derived ceramics (PDCs), as the name suggests, refer to ceramics, mostly silicon-based, that are derived from polymers through a series of transformative steps [26]. While the advent of PDCs commenced with the use of molecular precursors to produce non-oxide ceramics [26–28], practical polymer-to-ceramic transformation of silicon-based polymers was first reported in the 1970s [26, 29]. Presence of strong bonds between different constituent elements in these precursors enables the synthesis of multinary ceramics [26, 30, 31] that cannot be obtained via conventional routes. Such multinary ceramics can be categorized as

Fig. 11.2 Steps associated with PDC route (based on [26, 30])

binary (SiC and BN), ternary (such as SiOC and SiCN), and quaternary (such as SiOCN, SiBCN, and SiAlOC) systems [26]. Recent times have also witnessed successful attempts at incorporating new elements, such as Zr and Hf in PDCs [32, 33], thereby expanding the range to pentanary ceramic systems.

An interesting facet of PDCs is the ability to synthesize ceramics via bottom-up route with precise control of microstructure, chemical composition, and phase distribution via careful selection of polymeric precursors and process parameters [26, 30]. Such precise control helps in obtaining tunable properties of the final ceramic, be it mechanical, electrical, thermal, or chemical. Moreover, ceramics processed via PDC route offer two significant advantages over ceramics produced using conventional route. First, it offers the scope for synthesizing ceramics at lower temperatures, such as SiC and Si_3N_4 — at up to 1000 °C via PDC route vis-à-vis at 1700–2000 °C via powder metallurgy route [26]. Second, ceramics synthesized via PDC route exhibit higher thermal stability and better mechanical properties (such as oxidation and creep resistance) compared to those via conventional routes [34, 35]. For instance, polymer-derived SiBCN has been reported to remain stable till 2200 °C in non-oxide atmosphere due to the dominance of kinetics over thermodynamics of phase transformation [26, 36].

In terms of processing, PDCs are produced from polymeric precursors through a series of steps as shown in Fig. 11.2.

After shaping, these precursors undergo cross-linking at lower temperatures (up to 200 °C) [26, 30]. Cross-linked polymer is subsequently pyrolyzed at higher temperatures ($\geq$1000 °C) in inert (non-oxide) atmosphere, enabling its conversion to a ceramic (inorganic species) via loss of organic moieties [26, 30]. Often, fillers are added prior to ceramization (pyrolysis of polymer) in order to reduce both porosity and shrinkage caused by the loss of such moieties [26, 37]. Table 11.2 shows major polymeric precursors used to synthesize commonly processed PDCs.

In terms of microstructure, PDCs undergo phase evolution as a function of ceramization (pyrolysis) temperature [26, 30]. When pyrolyzed at lower temperature (800–1200 °C), PDCs consist of an amorphous matrix that is coupled with "free" carbon phase where carbon atoms are bonded to each other (but not to silicon) in graphite-like structure. With increase in ceramization temperature (>1200 °C), PDCs exhibit localized molecular rearrangement, resulting in phase separation in the amorphous matrix (such as the amorphous matrix in SiCN separating into SiC and Si_3N_4 phases), followed by the crystallization of separated phases [26, 30]. Further increase in crystallized content is observed with increase in ceramization temperature, which later decomposes to release gaseous by-products (such as CO_2) [26, 30].

Table 11.2 List of common polymeric precursors used for producing commonly processed PDCs (based on [26, 30, 32, 33])

PDC system	Polymeric precursors
SiOC	Polysiloxanes
SiCN	Polyorganosilazanes
	Polysilylcarbodiimides
SiBCN	Borazines
	Polyborosilazanes
	Polyborosilylcarbodiimides
SiBOC	Polyorganoborosiloxane
SiAlOC	Polyaluminosiloxane
SiHfCNO	Polysilazane and Hafnium tetra (*n*-butoxide)
$SiOC/ZrO_2$	Polymethylsilsesquioxane and Zirconium tetra (*n*-propoxide)

The combination of amorphous matrix and free carbon phase resembles the "phonon-glass electron-crystal" (PGEC) structure—the desired structure of an ideal TE material as hypothesized by Slack [38]. This hypothesis is based on the premise that while phonon glass ensures low κ (due to low κ_L as a result of its amorphous nature), the electron crystal exhibits high σ, typical of a single crystal. Thus, the thermoelectric potential of PDCs stems from its resemblance to PGEC structure, as "free" carbon phase could exhibit σ similar to graphite, while the bulk amorphous matrix could lead to low κ. Such potential of PDCs, coupled with other critical properties, such as excellent thermal and chemical stability, exceptional creep resistance till ~1500 °C, abundance of constituent elements, and relatively higher eco-friendliness compared to existing thermoelectrics, enhances the possibility of application for commercial purposes [26, 39–41]. This spawns interest in exploring and analyzing the possibility and means of developing PDCs as an alternative TE material.

Yet, barring one research work [25], no single study has been undertaken on the simultaneous analysis of all three TE properties (κ, σ, and S) of any single PDC system. However, individual studies have focused on measuring only one or two of these properties for the analyzed PDC. In the following section, a detailed discussion is presented on the literature published in this regard for different PDC systems.

11.3 Polymer-Derived Ceramics: Thermoelectric Properties

11.3.1 Electrical Conductivity (σ)

Among all the three thermoelectric properties, electrical conductivity (σ) remains the most highly explored property for PDCs. Table 11.3 shows the values of σ that have been measured for various PDC systems.

Table 11.3 Electrical conductivity (σ) of different PDC systems

PDC system	σ (S/cm)	Measurement temperature	Refs.
SiOC	10^{-12} to 10^{0}	20–1500 °C	[25, 37, 39–59]
Filled SiOC	10^{-5} to 10^{3}	20–1400 °C	
SiCN	10^{-10} to 10^{0}	20–1000 °C	[60–75]
Filled SiCN	10^{-8} to 10^{2}	20 °C	
SiOCN	10^{-5} to 10^{-1}	20–800 °C	[53–55]
SiBCN	10^{-13} to 10^{-1}	20–450 °C	[68–70, 76, 77]
SiAlCO	10^{-11} to 10^{-1}	20–300 °C	[78, 79]
SiBOC	10^{-5} to 10^{-3}	20 °C	[80]
SiCN(H)	10^{-7} to 10^{1}	50–400 °C	[81]

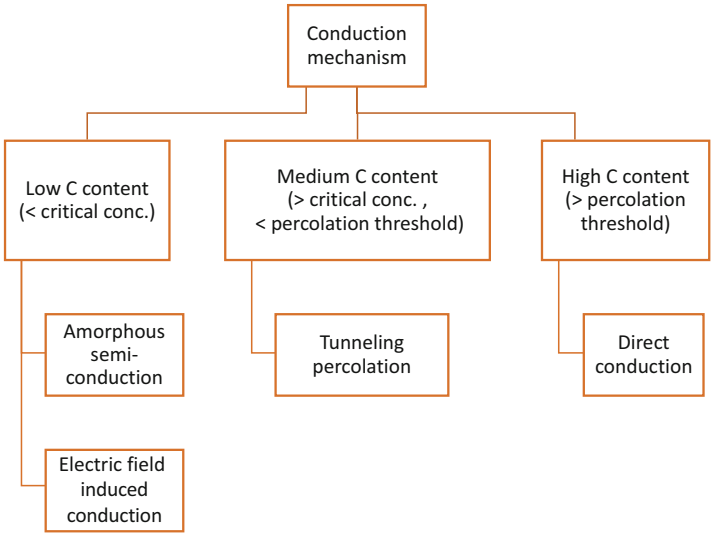

Fig. 11.3 Mechanisms/Regimes of PDCs electrical conduction: regimes

As is evident from data in Table 11.3, σ of any PDC varies over a wide range from the insulating regime (<10^{-6} S/cm) to the semiconducting regime (10^{-6} to 10^{3} S/cm), indicating that it can be tuned to desired values. For all the aforementioned PDC systems that are listed in Table 11.3, σ values, as well as the underlying conduction mechanism, are both observed to vary primarily with the amount of graphitic-like free carbon content present. This variation, both in values and mechanism of electrical conduction, can be categorized into three groups or regimes that are shown in Fig. 11.3.

The first regime corresponds to high levels of free carbon content, where the graphitic-like phase is beyond percolation threshold, and is, therefore, continuous throughout the concerned PDC. Interestingly, such percolation threshold for free carbon phase can be as low as 5 vol. % [56], with the phase continuity enabling seamless movement of charge carriers across the specimen, thus resulting in higher symbol for electrical conductivity via direct conduction mechanism in the

aforementioned PDC system [25, 26, 53, 63, 70, 82]. For instance, general effective media (GEM)-based modeling indicates higher σ for SiOC ($\geq 10^{-2}$ S/cm) with low percolation threshold (5 vol. %) when compared to that of SiOC ($\sigma = 10^{-10}$ to 10^{-8} S/cm) with higher percolation threshold (20 vol. %) [56]. This has also been observed for SiOC elsewhere, with lower electrical resistivity seen for SiOC ceramized at higher temperature (0.14 Ohm×m at 1400 °C vis-à-vis 0.35 Ohm×m at 1100 °C) on account of the formation of percolating network of turbostratic carbon [46]. Similar findings have been reported for polysilazane-derived SiCN that shows higher ($\sigma \sim 10^{-2}$ S/cm) due to the presence of percolating free carbon network [71].

On the other hand, the second regime focuses on PDCs where the graphitic-like carbon content is in the medium range, i.e., it is below percolation threshold and is, therefore, not entirely continuous, but it is not so low as to be fully discontinuous [26, 56, 71]. In this regime, free carbon phase is also surrounded by another (other) phase(s) present in the concerned PDC. Usually, this "other phases" refer to the amorphous matrix that exhibits lower σ values vis-à-vis free carbon network, thereby acting as a barrier to the movement of charge carriers [26, 30]. However, this amorphous barrier is quite thin, resulting in easy tunneling of charge carriers through it to hop across the specimen or move along the free carbon phase (in local regions where it is continuous) [60, 64, 71, 79, 83]. This mechanism is termed "tunneling percolation", which combines the "tunneling" of electrons across the amorphous barrier with the movement of charge carriers across the incomplete network of percolated free carbon.

Unlike the direct conduction mechanism, tunneling percolation corresponds to lower σ values. For example, SiOC shows lower ($\sigma = 10^{-12}$ to 10^{-3} S/cm), corresponding to the tunneling percolation regime when ceramized at lower temperatures, but exhibits higher ($\sigma \geq 10^{-2}$ S/cm) via direct conduction at higher temperatures [56]. Similarly, SiCN exhibits lower the symbol for electrical conductivity in the tunneling percolation regime (10^{-7} to 10^{-3} S/cm) vis-à-vis direct conduction regime ($\sigma = 10^{-3}$ to 10^{-2} S/cm) [56, 71, 72]. This can be easily understood as reduction in conductivity due to the emergence of discontinuity in free carbon network, which cannot be fully compensated by tunneling of electrons across the thin amorphous matrix.

Finally, the third regime is associated with PDCs that contain low levels of free carbon content, i.e., the amount of free carbon phase is below a critical concentration limit that enables tunneling of charge carriers across the amorphous matrix despite discontinuity in this phase [60, 79]. Hence, the barrier (amorphous matrix) between free carbon clusters is so thick that it is not possible for charge carriers to tunnel across it to other free carbon clusters across PDC specimen. As a result, PDCs in this regime exhibit much lower values of σ when compared to the aforementioned regimes. An example of this is SiCN that shows much lower ($\sigma = 10^{-9}$ to 10^{-6} S/cm) due to low amount of free carbon content—an outcome of lower ceramization temperature [60]—when compared to σ of SiCN in other studies mentioned earlier.

Unlike the first two regimes, electrical conduction in PDCs in this regime (i.e., low free carbon content) occurs via two mechanisms. The first mechanism is amorphous semiconduction, which arises because of the presence of dangling

carbon atoms in the amorphous matrix [53, 63, 71, 81, 84]. These atoms are like defect dopants that both provide charge carriers (electrons) and also give rise to energy states between valence and conduction bands in the amorphous matrix, resulting in the bandgap transforming into mobility gap [53, 63]. Hence, charge carriers can easily occupy and hop across these energy states, allowing for electron movement across the specimen and giving rise to electrical conductivity [53, 63, 82, 85, 86]. Simultaneously, free carbon atoms are also hypothesized to generate electric field within PDC specimen at low concentrations [60]. This is expected to improve electrical conductivity in the thick barrier region (amorphous matrix) between free carbon clusters, thereby easing the movement of charge carriers and enabling electrical conduction in PDCs that have low free carbon content.

Thus, encompassing all three regimes, electrical conductivity, both in terms of its magnitude and mechanism, is strongly impacted by the amount of free carbon content present in the concerned PDC. However, free carbon content is itself dependent primarily on processing temperature. Additionally, σ is also dependent on the filler used, as well as to some extent on the measurement temperature. All these aspects are discussed in some detail in the corresponding subsections.

Effect of Processing Temperature

Of the aforementioned critical parameters, the most commonly analyzed parameter is processing temperature that refers to either of ceramization, sintering, hot-pressing, or annealing temperature, as the case may be. For almost all studies mentioned in Table 11.3, increase in processing temperature results in increase in σ, as can be seen in Fig. 11.4 for a variety of PDC systems [39, 60, 68, 79].

As can be seen in Fig. 11.4a-d, graphs between electrical conductivity and the reciprocal of processing temperature indicate Arrhenius relationship between these two parameters [39, 60, 68, 79]. This is explained by the relationship between processing temperature and free carbon content, which influences electrical conductivity. Initially, increase in processing temperature leads to enhancement in free carbon content due to the conversion of sp^3-hybridized carbon atoms (present in amorphous matrix) to sp^2-hybridized carbon atoms (that become a part of the graphitic-like free carbon phase) [39, 42, 55, 61, 63, 83]. This increase in free carbon content results in an increase in σ, since free carbon phase is similar to graphite, and is, therefore, a good electrical conductor. This hypothesis is backed by the similarity in activation energies of the Arrhenius relationship between σ and processing temperature with that for the conversion of sp^3-hybridized carbon to sp^2-hybridized carbon (~3.5 eV) [55, 60, 68, 87]. Thus, initial enhancement in processing temperature improves σ of PDCs via increase in free carbon content.

However, subsequent increase in processing temperature influences the nature of both phases in PDCs (i.e., amorphous matrix and free carbon). Free carbon phase undergoes transformation from amorphous to nanocrystalline state, followed by in-plane growth of these nanocrystal clusters [40, 60, 79]. This can be seen in Fig. 11.5, which shows the cluster size of free carbon as a function of processing temperature for SiAlCO [79] and SiCN [83].

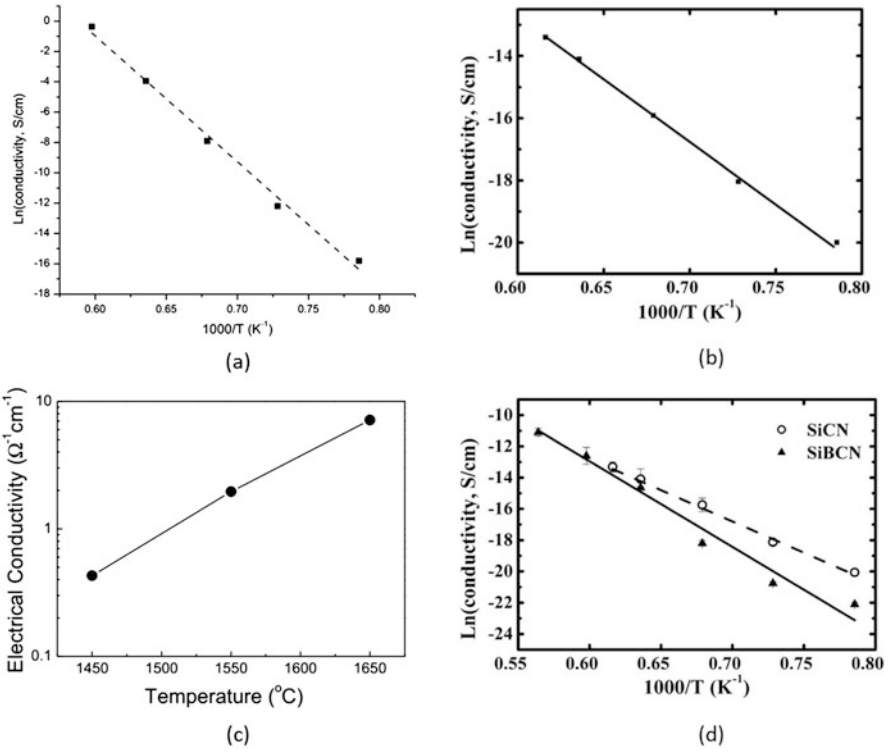

Fig. 11.4 Electrical conductivity as a function of (**a**) ceramization temperature for SiAlCO ceramics (reproduced from [79]); (**b**) ceramization temperature for SiCN ceramics (reproduced from [60]); (**c**) hot-pressing temperature for SiOC ceramics (reproduced from [39]); and (**d**) ceramization temperature for SiCN and SiBCN ceramics (reproduced from [68])

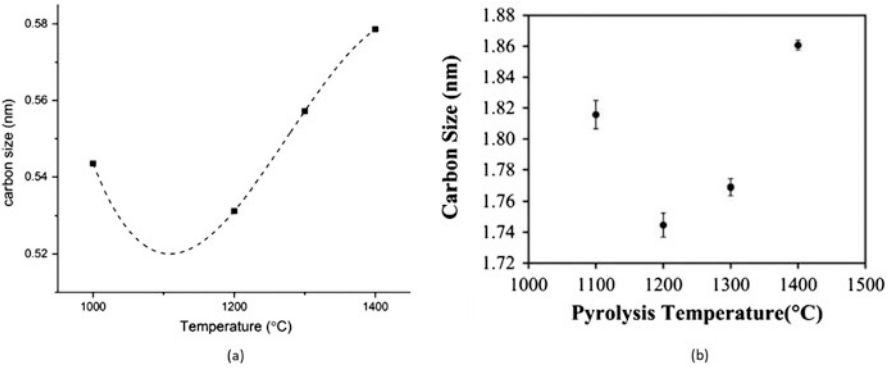

Fig. 11.5 Carbon size as function of ceramization temperature for (**a**) SiAlCO ceramic (reproduced from [79]) and (**b**) SiCN (reproduced from [83])

As can be seen for both PDCs, free carbon cluster size initially shows a decrease, which can be explained by the shift from amorphous state (i.e., distorted aromatic rings) to nanocrystalline state (i.e., regular six-membered rings) [88–90]. Subsequently, in-plane growth of these clusters results in an increase in cluster size, as well as the crystallite size of this phase, thereby reducing electron scattering and simultaneously enhancing electrical conductivity [79, 88, 89]. However, other studies highlight that it is not necessary for all PDCs to exhibit both the initial decrease and subsequent increase in cluster size, but instead show only one of these two phenomena [42, 43, 91]. This may be related to the nature of polymeric precursors used and/or processing conditions employed.

The increase in crystallinity of free carbon is also indicated by the emergence of a sharp peak at ~26.5° in X-ray diffraction (XRD) spectra of PDCs (Fig. 11.6b, e) that corresponds to crystalline graphite [42, 43, 46, 50]. However, this increase in crystallinity and cluster size of free carbon upon increase in processing temperature is simultaneously accompanied by the transformation of amorphous matrix to crystalline phases [25, 40, 42, 43, 46, 49, 80, 84, 92]. For instance, SiOC ceramics exhibit phase separation in amorphous matrix, whereby amorphous phases (such as SiC and SiO_2) separate from the matrix and crystallize subsequently with increase in processing temperature [40, 42, 43, 46, 93]. Such crystallization, especially in case

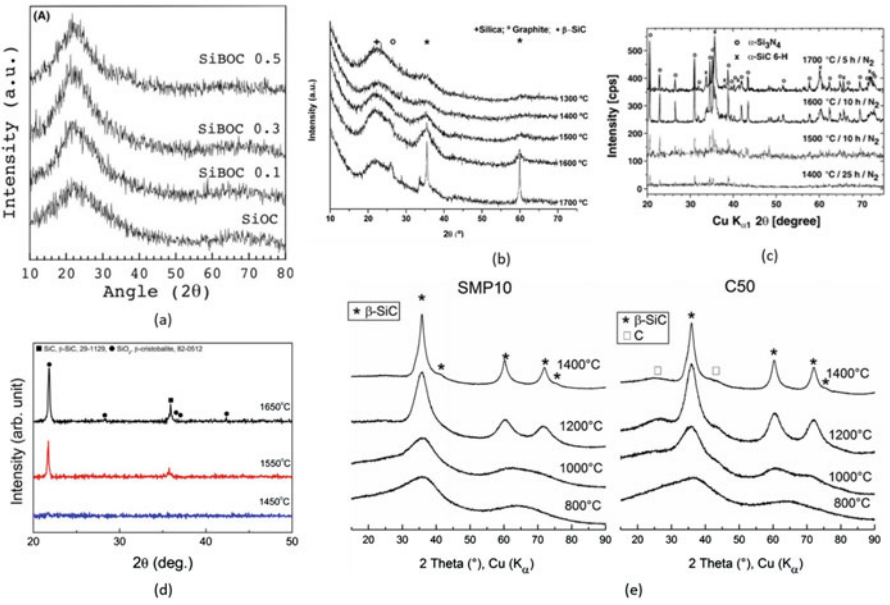

Fig. 11.6 XRD spectra of (**a**) SiOC and SiBOC samples ceramized at 1200 °C (reproduced from [80]); (**b**) SiOC sintered via spark plasma sintering at 1300, 1400, 1500, 1600, and 1700 °C (reproduced from [42]); (**c**) SiCN ceramics annealed at temperatures of 1400, 1500, 1600, and 1700 °C (reproduced from [84]); (**d**) SiOC + 1 mol.% Ba hot-pressed at 1450, 1550, and 1650 °C (reproduced from [40]); and (**e**) SiOC ceramized at temperatures of 800, 1000, 1200, and 1400 °C (reproduced from [43])

of SiC via reaction of Si with some amount of free carbon, leads to significant reduction in free carbon cluster size [25, 94]. However, its consequences on σ are not entirely clear or consistent, for while reduction in cluster size can lead to decrease in σ, formation of crystalline SiC, that possesses good thermal and electrical properties, is expected to enhance σ of PDCs.

The aforementioned increase in free carbon content with increase in processing temperature causes also change in the mechanism of electrical conduction, which can be understood by analyzing the behavior between σ and measurement temperature of the concerned PDC [25, 44, 54, 55, 69, 70, 81]. At lower processing temperatures, it is observed that σ of PDCs follows the relationship given by Eq. (11.5), where T_0 is constant, and T is measurement temperature[1] [56, 81]. Conversely, at higher processing temperatures, it is observed that $\sigma(T)$ of PDCs follows the relationship given by Eq. (11.6), where E_a is activation energy and k_B is Boltzmann constant [56, 81].

$$\sigma \sim e^{\left(-\frac{T_0}{T^{1/4}}\right)}, \tag{11.5}$$

$$\sigma \sim e^{\left(-\frac{E_a}{k_B T}\right)}, \tag{11.6}$$

For instance, methylvinyldichlorosilane-derived SiCN shows the relationship corresponding to Eq. (11.5) at processing temperatures of 775–1200 °C while exhibiting the relationship corresponding to Eq. (11.6) at higher processing temperatures [81] (as shown in Fig. 11.7).

The first relationship (Eq. (11.5)) was earlier attributed to Mott's variable range hopping (VRH) behavior [44, 69, 70, 81] but has been later ascribed to band range hopping (BRH) behavior in subsequent studies [53]. Both hopping mechanisms are characteristic of amorphous semiconductors as these mechanisms indicate localized transfer of charge carriers, thereby highlighting lower free carbon content in the given ceramic [95–97]. This is in sync with existing literature that shows increase in free carbon content with rise in processing temperature, as discussed earlier. Thus, methylvinyldichlorosilane-derived SiCN exhibits hopping conduction due to lower free carbon content at lower processing temperature, as can be seen in Fig. 11.7a [81], while similar findings are also reported elsewhere for SiCN in other studies [69, 70], SiOCN [53], and SiOC [25].

On the other hand, the second relationship (Eq. 11.6) can be ascribed to a combination of two factors: one, increased ability of charge carriers to tunnel across excited energy states, and two, greater probability of charge carriers getting enough excitation energy to occupy energy states in conduction band [56, 81]. While the first

[1]Measurement temperature is not the same as processing temperature – processing temperature refers to the temperature at which the polymer is converted or sintered or annealed to obtain the ceramic, while measurement temperature refers to the temperature at which the concerned property of the ceramic is measured.

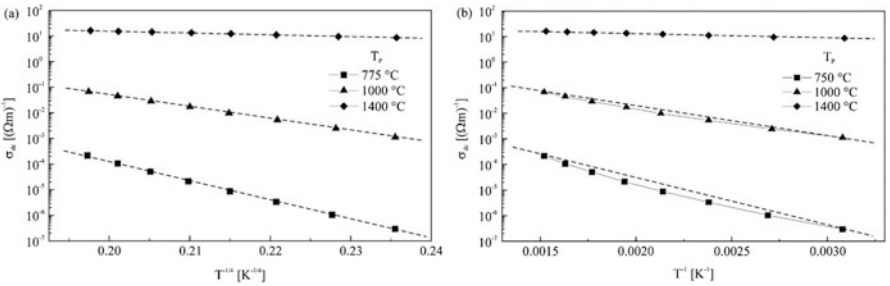

Fig. 11.7 Variation in σ as function of (**a**) $T^{1/4}$ and (**b**) T^{-1} for SiCN ceramics processed at three temperatures (775/750, 1000, and 1400 °C) (reproduced from [81])

factor is indicative of tunneling percolation mechanism, the second factor is associated with a fully percolated and continuous network of free carbon [56, 81]. Thus, increase in processing temperature can be said to significantly augment free carbon content levels, such that this leads to change in the conduction mechanism of final ceramic, and thereby, improve σ. This can be seen in case of methylvinyldichlorosilane-derived SiCN that shows much higher σ at processing temperature of 1400 °C (compared to 775/750 and 1000 °C), even at lower measurement temperatures (Fig. 11.7b) [81]. Again, similar observations have also been made for other PDC systems, such as SiOC [44] and SiOCN [54]. Thus, for a number of PDCs, increase in ceramization temperature leads to increase in σ (via augmenting free carbon content), as well as variation in the associated conduction mechanism. However, it is not necessary that all PDCs exhibit both these relationships (Eqs. (11.5)–(11.6)) with increase in processing temperature – some PDCs may show only one of these two relationships [44].

Effect of Polymeric Precursor

Polymeric precursors remain another key determining factor behind both the amount of free carbon content and the resultant σ of concerned PDC. Mostly, this can be ascribed to the amount of carbon in polymer and its subsequent effect on free carbon content in the final ceramic. For instance, SiOCN obtained using polysilazane shows lower σ compared to SiOCN obtained using trione (amine) [55]. This is partly explained by the higher amount of carbon content in trione (precursor) that in turn enhances free carbon content in the final ceramic. Similar variation is observed in σ of SiOC, with higher σ observed for SiOC derived from polymeric precursors with high carbon content [58].

Effect of Filler

In addition to processing temperature and polymeric precursor, the nature and amount of filler used play also a vital role in influencing σ of the final ceramic. Fillers are often used to reduce the porosity attained often during polymer-to-ceramic transformation, thereby enhancing the density of final ceramic [37]. Use of conductive fillers enhances σ of the ceramic mostly via enabling the formation of percolation paths that may also interact with the free carbon phase, even at low concentrations of these fillers [37, 52, 64, 83].

For instance, the inclusion of graphitic oxide (GO) as filler in (polysiloxane) SILRES62-derived SiOC (with the use of polyvinyl alcohol or PVA) is reported to form percolation networks even at very low filler concentration (<2 wt. %), thereby enhancing its σ [52]. This is attributed to the occurrence of GO-induced crystallization of graphite that improves σ of free carbon phase, and, thereby, of the final ceramic. Similarly, the formation of percolation network of $MoSi_2$ is responsible for significant rise in σ of polymethylsiloxane-derived SiOC, even when free carbon content is low (at temperatures below 1200 °C) [37]. However, unlike GO, $MoSi_2$ does not induce precipitation or crystallization of free carbon till 1200 °C [37]. Other PDC systems are also reported to exhibit significant rise in σ upon the incorporation of conductive fillers at low concentrations due to the formation of percolation network, such as CNT (<1 vol. %) [67] and reduced graphene oxide (0.2 wt. %) [72] in SiCN. As in case of $MoSi_2$, these fillers have not been observed to induce any significant extent of crystallization of free carbon phase in SiCN ceramics, and thus, increase in σ is solely due to the introduction of well-dispersed conductive filler in the ceramic. Interestingly, the use of higher concentrations of such conductive fillers (beyond the percolation threshold) does not cause any drastic improvement in σ of the ceramic, such as in case of CNT [67] and reduced graphene oxide [72] in SiCN. This is reported to be possibly due to the agglomeration or random dispersion of filler in the concerned ceramic.

11.3.2 Thermal Conductivity (κ)

Thermal conductivity (κ) of any material is strongly associated with two aspects: its nature (crystalline or amorphous material, along with grain/crystal size) and presence of defects (such as porosity) [98, 99]. With regard to PDCs, κ has not been studied to the extent to which σ has been explored. Yet, of the limited attempts undertaken in this regard, the first two aspects (nature of material and porosity) have been observed to be critical to κ of PDCs, both at room and high temperatures.

The importance of the nature of the concerned PDC can be understood via analyzing changes observed in its microstructure with increase in processing temperature. As described earlier, PDCs consist of two phases (amorphous matrix and free carbon phase) at lower processing temperatures [26, 30]. Of these phases, while

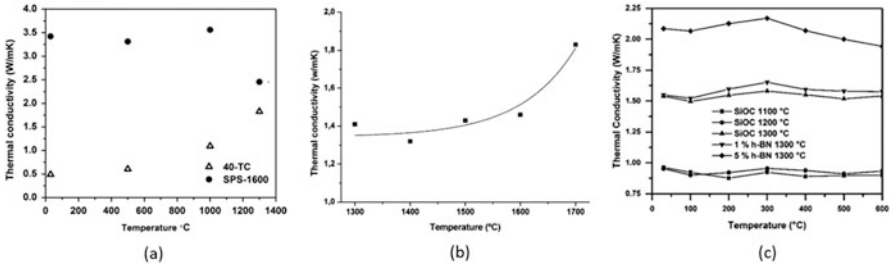

Fig. 11.8 Thermal conductivity (**a**) as a function of measurement temperature for SiBCN foam and SPS sample (reproduced from [98]); (**b**) as a function of sintering temperature for SPS SiOC (reproduced from [47]); (**c**) as a function of measurement temperature for SPS SiOC sintered at different temperatures (reproduced from [25])

free carbon phase is thermally conductive, the amorphous matrix is thermally insulating as it can scatter phonons and, thereby, reduce thermal conductivity of the final ceramic. However, subsequent increase in processing temperature causes crystallization of both amorphous matrix and free carbon phases, thereby transforming the nature of the ceramic (from amorphous to crystalline). Further, increase in ceramization temperature enables better flow of viscous matrix, thereby enabling better reduction in porosity of the material. This in turn is expected to improve κ of the concerned PDC system, and the same has been reported in several studies.

For instance, SiBCN foam shows lower κ compared to SiBCN processed using spark plasma sintering (SPS) (Fig. 11.8a), since the foam is completely amorphous and contains pores, while SPS sample is crystalline in nature and is highly dense [91]. This trend (of lower κ for foam vis-à-vis SPS sample) is observed even with increase in measurement temperature from RT to 1300 °C (Fig. 11.8a). On the other hand, another study highlights increase in κ of SiOC with increase in SPS (processing) temperature, with a significant amount of jump in κ observed during the increase in SPS temperature from 1600 °C to 1700 °C (Fig. 11.8b) [42]. The initial limited increase is ascribed to the interruption of amorphous matrix with crystallites of β − SiC and free carbon phase (that is segregated). However, the subsequent dramatic jump in κ with increase in SPS temperature from 1600 °C to 1700 °C is attributed to the significant increase in size of β − SiC crystallites and carbon clusters. Similar increase in κ with increase in processing temperature is also observed for SiOC elsewhere, and is explained by the formation of SiC via carbothermal reduction (Fig. 11.8c) [25].

An interesting aspect with regard to all these studies is the enhanced contribution of crystalline phases (especially β−SiC), obtained via phase separation from the amorphous matrix for the aforementioned PDC systems. In contrast, the contribution of free carbon phase to improving κ of these ceramics appears to be quite limited, even with significant increase in processing temperature [25, 42]. This may be

Table 11.4 Thermal conductivity of PDC systems

PDC system	Thermal conductivity, κ, $W \times m^{-1} \times K^{-1}$	Measurement temperature	Refs.
SiOC	0.027–2.7 (pure) 1.7–5.6 (upon addition of fillers or reinforcements)	20–1300 °C	[25, 40, 42, 92, 94, 100, 101, 103]
SiCN	2.1–5.5 (from pure to addition of fillers and reinforcements)	100–900 °C	[102]
SiBCN	0.647–3.5 (pure) 0.5–2.0 (with sago as filler)	20–1300 °C	[91, 104]

Table 11.5 Seebeck coefficient values

PDC system	S, μV/K	Range of measurement temperature, °C and K	Refs.
SiCN	−10	Room temperature (20 °C, 293 K)	[63]
SiOC	−10 to −12	30–150 °C (303–453 K)	[25]
SiOC/h − BN	−33		
SiBCN	0–2	−223 to 27 °C (50–300 K)	[63, 70]

possibly due to the lack of a fully continuous percolating structure of free carbon phase for these PDC systems.

With regard to measurement temperature, PDCs show a contrasting trend for κ across existing literature (Fig. 11.8). For instance, studies show invariant κ at low measurement temperatures ($\leq$1000 °C) for SiOC [25, 100, 101], as well as for SiBCN [91], but also highlight that SiBCN shows variation in κ at higher measurement temperatures (>1000 °C). The latter trend is partly explained by the role of higher crystallinity for SiBCN sample, since crystalline materials tend to exhibit reduction in κ via enhanced phonon scattering with increase in measurement temperature. However, this explanation is complemented with speculation regarding the exact role of SiO_2- a phase observed in SiOC but found absent in non-oxide PDCs- that remains to be fully analyzed and understood [25]. Finally, PDCs also exhibit significant increase in κ upon incorporation of conductive fillers, such as CNT in SiCN [102] and Ba in SiOC [40], especially with increase in measurement temperature. While CNT forms a strong percolating network in the ceramic that enables electrons to participate in conduction, and, thereby, enhance κ of SiCN, presence of Ba enables the formation of percolating network of free carbon and its association with $\beta-$SiC crystallites to improve κ of SiOC [40, 102].

Table 11.4 shows thermal conductivity of different PDC systems studied till date.

11.3.3 Seebeck Coefficient (S)

Seebeck coefficient (S) of PDC systems has been reported or analyzed only in three studies, among which two report values for SiCN/SiBCN systems [63, 70], while the

third has reported *S* for SiOC [25]; these values are provided in Table 11.5. Additionally, the third study [25] also reports *S* of SiOC filled with hexagonal boron nitride (*h−BN*), and these values are also given in Table 11.5.

As can be seen, while SiOC and SiCN exhibit *S* in the range from −10 to −12 μV/K, SiBCN shows much lower *S* (up to 2 μV/K). The lower value of *S* for SiBCN (compared to SiCN) is ascribed to the respective behavior of boron (B) and nitrogen (N) as *p*- and *n*-type dopants, in the SiC network [105]. Addition of B is explained in this study to create holes that compensate for additional electrons introduced in SiC network via incorporation of N (*n*-type dopant). With regard to SiOC, its *S* shows marginal increase in absolute value from −10 to −12 μV/K with increase in temperature from 303 K to 423 K. This behavior is understood as the outcome of interactions between electrons (hopping across free carbon phase) and phonons (transferring in the amorphous phase) [25]. Interestingly, addition of *h−*BN is observed to enhance *S* of SiOC at all temperatures in the same study [25] while also causing difference in Seebeck behavior of *h−*BN-filled SiOC vis-à-vis pure SiOC. This difference, whereby *h−*BN-filled SiOC shows initial decrease in *S* followed by its subsequent increase with rise in measurement temperature, is attributed to the wide bandgap of *h−*BN [25, 106]. However, the same study points out the need for more research to assess the contribution of amorphous matrix to *S* values of PDCs.

Interestingly, the last study [25] also highlights simultaneous increase in both *S* and σ of SiOC with increase in measurement temperature. This is attributed to the occurrence of electrical conduction in PDCs via hopping of charge carriers [53, 63]. Also, anomaly is observed in the nature of charge carriers as indicated by *S* and Hall effect [25, 51], which is explained by localization of charge carriers due to hopping conduction [107]. Given the importance of hopping as a mechanism for electrical conduction in PDCs (as discussed earlier), similar findings may be reported in future for other PDC systems.

11.4 Summary and Future Work

A vast majority of initiatives directed toward the development of high ZT materials have focused solely on engineering the crystal structure of highly crystalline materials while completely ignoring amorphous materials due to inherent poor electrical conductivity. In contrast, despite the amorphous nature, PDCs exhibit electrical conductivity in the semiconducting regime along with intrinsically poor thermal conductivity (<2.5 $W \times m^{-1} \times K^{-1}$). This behavior offers a strong platform for considering PDCs as a potential thermoelectric material that exhibits "phonon-glass electron-crystal" behavior. This potential is significantly enhanced by the observation of simultaneous increase in electrical conductivity and Seebeck coefficient of these PDCs with increase in measurement temperature. However, given the low values for both parameters, this potential for PDCs needs to be further explored on a sustained basis, especially with regard to Seebeck effect that continues to remain

much of an enigma till date, particularly at higher temperature regimes. This is critical in order to develop mechanisms that can help enhance both Seebeck coefficient and ZT values of PDCs. Further research works also needs to be undertaken on studying thermoelectric properties of any PDC that is processed under the same conditions for developing better understanding of process-property relationship, especially, regarding the impact of variation in prominent parameters, such as polymeric precursor, chemical composition of ceramic, processing temperature, and free carbon content, on thermoelectric properties of various PDC systems. Such research remains pivotal to harnessing the true potential of PDCs for commercial thermoelectric applications.

Acknowledgments The authors would like to acknowledge the financial support by Robert Patrick Jenkins Professorship and Dean's Faculty Fellow Professorship. A.B.K would like to acknowledge the financial support provided through the scholarship fund of Southern Automotive Women's Forum.

References

1. K. Biswas, J. He, I.D. Blum, C.-I. Wu, T.P. Hogan, D.N. Seidman, et al., High-performance bulk thermoelectrics with all-scale hierarchical architectures. Nature **489**, 414–418 (2012). https://doi.org/10.1038/nature11439
2. C.B. Vining, An inconvenient truth about thermoelectrics. Nat. Mater. **8**, 83–85 (2009). https://doi.org/10.1038/nmat2361
3. T.M. Tritt, M.A. Subramanian, Thermoelectric materials , phenomena, and applications: a bird's eye view. MRS Bull. **31**, 188–198 (2006). https://doi.org/10.1557/mrs2006.44
4. J.P. Heremans, M.S. Dresselhaus, L.E. Bell, D.T. Morelli, When thermoelectrics reached the nanoscale. Nat. Nanotechnol. **8**, 471–473 (2013). https://doi.org/10.1038/nnano.2013.129
5. L.D. Hicks, M.S. Dresselhaus, Effect of quantum-well structures on the thermoelectric figure of merit. Phys. Rev. B **47**, 12727–12731 (1993). https://doi.org/10.1103/PhysRevB.47.12727
6. L.D. Hicks, M.S. Dresselhaus, Thermoelectric figure of merit of a one-dimensional conductor. Phys. Rev. B **47**, 16631–16634 (1993). https://doi.org/10.1103/PhysRevB.47.16631
7. A. Mehdizadeh Dehkordi, M. Zebarjadi, J. He, T.M. Tritt, Thermoelectric power factor: enhancement mechanisms and strategies for higher performance thermoelectric materials. Mater. Sci. Eng. R Rep. **97**, 1–22 (2015). https://doi.org/10.1016/j.mser.2015.08.001
8. M. Zebarjadi, K. Esfarjani, M.S. Dresselhaus, Z.F. Ren, G. Chen, Perspectives on thermoelectrics: from fundamentals to device applications. Energ. Environ. Sci. **5**, 5147–5162 (2012). https://doi.org/10.1039/C1EE02497C
9. S.I. Kim, K.H. Lee, H.A. Mun, H.S. Kim, S.W. Hwang, J.W. Roh, et al., Dense dislocation arrays embedded in grain boundaries for high-performance bulk thermoelectrics. Science **348**, 109–114 (2015). https://doi.org/10.1126/science.aaa4166
10. S. Wang, H. Li, R. Lu, G. Zheng, X. Tang, Metal nanoparticle decorated n-type Bi_2Te_3-based materials with enhanced thermoelectric performances. Nanotechnology **24**, 285702 (2013). https://doi.org/10.1088/0957-4484/24/28/285702
11. K.F. Hsu, S. Loo, F. Guo, W. Chen, J.S. Dyck, C. Uher, et al., Cubic AgPbmSbTe2+m: bulk thermoelectric materials with high figure of merit. Science **303**, 818–821 (2004). https://doi.org/10.1126/science.1092963

12. P.F.P. Poudeu, J. D'Angelo, A.D. Downey, J.L. Short, T.P. Hogan, M.G. Kanatzidis, High thermoelectric figure of merit and nanostructuring in bulk p-type Na1−xPbmSbyTem+2. Angew. Chem. Int. Ed. **45**, 3835–3839 (2006). https://doi.org/10.1002/anie.200600865
13. Y. Pei, J. Lensch-Falk, E.S. Toberer, D.L. Medlin, G.J. Snyder, High thermoelectric performance in PbTe due to large nanoscale Ag2Te precipitates and La doping. Adv. Funct. Mater. **21**, 241–249 (2011). https://doi.org/10.1002/adfm.201000878
14. A. Saramat, G. Svensson, A.E.C. Palmqvist, C. Stiewe, E. Mueller, D. Platzek, et al., Large thermoelectric figure of merit at high temperature in Czochralski-grown clathrate Ba[sub 8]Ga [sub 16]Ge[sub 30]. J. Appl. Phys. **99**, 023708 (2006). https://doi.org/10.1063/1.2163979
15. T. Caillat, J.-P. Fleurial, A. Borshchevsky, Preparation and thermoelectric properties of semiconducting Zn 4 Sb 3. J. Phys. Chem. Solid **58**, 1119–1125 (1997)
16. X. Shi, J.J. Yang, J.R. Salvador, M. Chi, J.Y. Cho, H. Wang, et al., Multiple-filled skutterudites: high thermoelectric figure of merit through separately optimizing electrical and thermal transports. J. Am. Chem. Soc. **133**, 7837–7846 (2011). https://doi.org/10.1021/ja111199y
17. L.-D. Zhao, S.-H. Lo, Y. Zhang, H. Sun, G. Tan, C. Uher, et al., Ultralow thermal conductivity and high thermoelectric figure of merit in SnSe crystals. Nature **508**, 373–377 (2014). https://doi.org/10.1038/nature13184
18. W. Liu, X. Tan, K. Yin, H. Liu, X. Tang, J. Shi, et al., Convergence of conduction bands as a means of enhancing thermoelectric performance of n-type Mg2Si(1-x)Sn(x) solid solutions. Phys. Rev. Lett. **108**, 166601 (2012). https://doi.org/10.1103/PhysRevLett.108.166601
19. X. Yan, W. Liu, H. Wang, S. Chen, J. Shiomi, K. Esfarjani, et al., Stronger phonon scattering by larger differences in atomic mass and size in p-type half-Heuslers Hf1−xTixCoSb0.8Sn0.2. Energ. Environ. Sci. **5**, 7543 (2012). https://doi.org/10.1039/c2ee21554c
20. X.W. Wang, H. Lee, Y.C. Lan, G.H. Zhu, G. Joshi, D.Z. Wang, et al., Enhanced thermoelectric figure of merit in nanostructured n-type silicon germanium bulk alloy. Appl. Phys. Lett. **93**, 193121 (2008). https://doi.org/10.1063/1.3027060
21. H. Liu, X. Shi, F. Xu, L. Zhang, W. Zhang, L. Chen, et al., Copper ion liquid-like thermoelectrics. Nat. Mater. **11**, 422–425 (2012). https://doi.org/10.1038/nmat3273
22. E.S. Toberer, C.A. Cox, S.R. Brown, T. Ikeda, A.F. May, S.M. Kauzlarich, et al., Traversing the metal-insulator transition in a Zintl phase: rational enhancement of thermoelectric efficiency in $Yb_{14}Mn_{1-x}Al_xSb_{11}$. Adv. Funct. Mater. **18**, 2795–2800 (2008). https://doi.org/10.1002/adfm.200800298
23. J.H. Sui, J.C.F. Li, J.Q. He, Y.-L.L. Pei, D. Berardan, H. Wu, et al., Texturation boosts the thermoelectric performance of BiCuSeO oxyselenides. Energ. Environ. Sci. **6**, 2916 (2013). https://doi.org/10.1039/c3ee41859f
24. NHTSA, CAFE - Fuel Economy. (National Highway Traffic Safety Administration, 2013), http://www.nhtsa.gov/fuel-economy/. Accessed 24 June 2016
25. A.B. Kousaalya, X. Zeng, M. Karakaya, T. Tritt, S. Pilla, A.M. Rao, Polymer-derived silicon oxycarbide ceramics as promising next-generation sustainable thermoelectrics. ACS Appl. Mater. Interfaces **10**, 2236–2241 (2018). https://doi.org/10.1021/acsami.7b17394
26. P. Colombo, G. Mera, R. Riedel, G. Domenicosorarù, Polymer-derived ceramics: 40 years of research and innovation in advanced ceramics. J. Am. Ceram. Soc. **93**, 1805–1837 (2010). https://doi.org/10.1111/j.1551-2916.2010.03876.x
27. F.W. Ainger, J.M. Herbert, The preparation of phosphorus-nitrogen compounds as non-porous solids, in *Spec. Ceram*, ed. by P. Popper, 1st edn., (Academic Press, New York, 1960), pp. 168–182
28. P.G. Chantrell, P. Popper, Inorganic polymers and ceramics, in *Spec. Ceram*, ed. by P. Popper, 1st edn., (Academic Press, New York, 1965), pp. 87–103
29. W. Verbeek, Production of shaped articles of homogeneous mixtures of silicon carbide and nitride. US3853567A, 1973

30. R. Riedel, G. Mera, R. Hauser, A. Klonczynski, Silicon-based polymer-derived ceramics: synthesis properties and applications-a review. J. Ceram. Soc. Jpn. **114**, 425–444 (2006). https://doi.org/10.2109/jcersj.114.425
31. E. Ionescu, G. Mera, R. Riedel, L.A. An, R. Riedel, C. Konetschny, et al., Polymer-derived ceramics (PDCs): materials design towards applications at ultrahigh-temperatures and in extreme environments. MAX Phases Ultra-High Temp. Ceram. Extrem. Environ. **81**, 203–245. https://doi.org/10.4018/978-1-4666-4066-5.ch007
32. R. Sujith, A.B. Kousaalya, R. Kumar, Coarsening induced phase transformation of hafnia in polymer-derived Si-Hf-C-N-O ceramics. J. Am. Ceram. Soc. **94**, 2788–2791 (2011). https://doi.org/10.1111/j.1551-2916.2011.04719.x
33. E. Ionescu, C. Linck, C. Fasel, M. Müller, H. Kleebe, R. Riedel, Polymer-derived SiOC/ZrO_2 ceramic nanocomposites with excellent high-temperature stability. J. Am. Ceram. Soc. **93**, 241–250 (2010). https://doi.org/10.1111/j.1551-2916.2009.03395.x
34. R. Kumar, F. Phillipp, F. Aldinger, Oxidation induced effects on the creep properties of nanocrystalline porous Si–B–C–N ceramics. Mater. Sci. Eng. A **445–446**, 251–258 (2007). https://doi.org/10.1016/J.MSEA.2006.09.024
35. N.V. Ravi Kumar, S. Prinz, Y. Cai, A. Zimmermann, F. Aldinger, F. Berger, et al., Crystallization and creep behavior of Si–B–C–N ceramics. Acta Mater. **53**, 4567–4578 (2005). https://doi.org/10.1016/J.ACTAMAT.2005.06.011
36. R. Riedel, A. Kienzle, W. Dressler, L. Ruwisch, J. Bill, F. Aldinger, A silicoboron carbonitride ceramic stable to 2,000°C. Nature **382**, 796–798 (1996). https://doi.org/10.1038/382796a0
37. J. Cordelair, P. Greil, Electrical characterization of polymethylsiloxane/MoSi2-derived composite ceramics. J. Am. Ceram. Soc. **84**, 2256–2259 (2004). https://doi.org/10.1111/j.1151-2916.2001.tb00998.x
38. G.A. Slack, New materials and performance limits for thermoelectric cooling, in *CRC Handbook of Thermoelectrics*, ed. by D. M. Rowe, 1st edn., (CRC Press, Boca Raton, FL, 1995), pp. 399–432
39. K.J. Kim, J.-H.H. Eom, Y.-W.W. Kim, W.-S.S. Seo, Electrical conductivity of dense, bulk silicon-oxycarbide ceramics. J. Eur. Ceram. Soc. **35**, 1355–1360 (2015). https://doi.org/10.1016/j.jeurceramsoc.2014.12.007
40. J.-H. Eom, Y.-W. Kim, K.J. Kim, W.-S. Seo, Improved electrical and thermal conductivities of polysiloxane-derived silicon oxycarbide ceramics by barium addition. J. Eur. Ceram. Soc. **38**, 487–493 (2018). https://doi.org/10.1016/J.JEURCERAMSOC.2017.09.045
41. M.A. Mazo, A. Nistal, A.C. Caballero, F. Rubio, J. Rubio, J.L. Oteo, Influence of processing conditions in TEOS/PDMS derived silicon oxycarbide materials. Part 1: microstructure and properties. J. Eur. Ceram. Soc. **33**, 1195–1205 (2013). https://doi.org/10.1016/J.JEURCERAMSOC.2012.11.022
42. M.A. Mazo, A. Tamayo, A.C. Caballero, J. Rubio, Electrical and thermal response of silicon oxycarbide materials obtained by spark plasma sintering. J. Eur. Ceram. Soc. **37**, 2011–2020 (2017). https://doi.org/10.1016/J.JEURCERAMSOC.2017.01.003
43. F. Dalcanale, J. Grossenbacher, G. Blugan, M.R. Gullo, A. Lauria, J. Brugger, et al., Influence of carbon enrichment on electrical conductivity and processing of polycarbosilane derived ceramic for MEMS applications. J. Eur. Ceram. Soc. **34**, 3559–3570 (2014). https://doi.org/10.1016/J.JEURCERAMSOC.2014.06.002
44. P. Moni, M. Wilhelm, K. Rezwan, The influence of carbon nanotubes and graphene oxide sheets on the morphology, porosity, surface characteristics and thermal and electrical properties of polysiloxane derived ceramics. RSC Adv. **7**, 37559–37567 (2017). https://doi.org/10.1039/C7RA01937H
45. M. Shibuya, M. Sakurai, T. Takahashi, Preparation and characteristics of a vapor-grown carbon fiber/ceramic composite using a methylsilicone precursor. Compos. Sci. Technol. **67**, 3338–3344 (2007). https://doi.org/10.1016/J.COMPSCITECH.2007.03.023
46. S. Martínez-Crespiera, E. Ionescu, H.-J. Kleebe, R. Riedel, Pressureless synthesis of fully dense and crack-free SiOC bulk ceramics via photo-crosslinking and pyrolysis of a

polysiloxane. J. Eur. Ceram. Soc. **31**, 913–919 (2011). https://doi.org/10.1016/j.jeurceramsoc.2010.11.019
47. G.M. Renlund, S. Prochazka, R.H. Doremus, Silicon oxycarbide glasses: part II. Structure and properties. J. Mater. Res. **6**, 2723–2734 (1991). https://doi.org/10.1557/JMR.1991.2723
48. A. Tamayo, M.A. Mazo, F. Rubio, J. Rubio, Structure properties relationship in silicon oxycarbide glasses obtained by spark plasma sintering. Ceram. Int. **40**, 11351–11358 (2014). https://doi.org/10.1016/J.CERAMINT.2014.03.111
49. W. Duan, X. Yin, Q. Li, X. Liu, L. Cheng, L. Zhang, Synthesis and microwave absorption properties of SiC nanowires reinforced SiOC ceramic. J. Eur. Ceram. Soc. **34**, 257–266 (2014). https://doi.org/10.1016/J.JEURCERAMSOC.2013.08.029
50. K. Lu, D. Erb, M. Liu, Thermal stability and electrical conductivity of carbon-enriched silicon oxycarbide. J. Mater. Chem. C **4**, 1829–1837 (2016). https://doi.org/10.1039/C6TC00069J
51. K.J. Kim, J.H. Eom, T.Y. Koh, Y.W. Kim, W.S. Seo, Effects of carbon addition on the electrical properties of bulk silicon-oxycarbide ceramics. J. Eur. Ceram. Soc. **36**, 2705–2711 (2016). https://doi.org/10.1016/j.jeurceramsoc.2016.04.034
52. C. Shen, E. Barrios, L. Zhai, Bulk polymer-derived ceramic composites of graphene oxide. ACS Omega **3**, 4006–4016 (2018). https://doi.org/10.1021/acsomega.8b00492
53. Y. Wang, T. Jiang, L. Zhang, L. An, Electron transport in polymer-derived amorphous silicon oxycarbonitride ceramics. J. Am. Ceram. Soc. **92**, 1603–1606 (2009). https://doi.org/10.1111/j.1551-2916.2009.03044.x
54. H.-Y. Ryu, Q. Wang, R. Raj, Ultrahigh-temperature semiconductors made from polymer-derived ceramics. J. Am. Ceram. Soc. **93**, 1668–1676 (2010). https://doi.org/10.1111/j.1551-2916.2010.03623.x
55. V.L. Nguyen, C. Zanella, P. Bettotti, G.D. Sorarù, Electrical conductivity of SiOCN ceramics by the powder-solution-composite technique. J. Am. Ceram. Soc. **97**, 2525–2530 (2014). https://doi.org/10.1111/jace.12963
56. J. Cordelair, P. Greil, Electrical conductivity measurements as a microprobe for structure transitions in polysiloxane derived Si–O–C ceramics. J. Eur. Ceram. Soc. **20**, 1947–1957 (2000). https://doi.org/10.1016/S0955-2219(00)00068-6
57. P. Colombo, T. Gambaryan-Roisman, M. Scheffler, P. Buhler, P. Greil, Conductive ceramic foams from preceramic polymers. J. Am. Ceram. Soc. **84**, 2265–2268 (2004). https://doi.org/10.1111/j.1151-2916.2001.tb01000.x
58. J. Kaspar, M. Graczyk-Zajac, S. Choudhury, R. Riedel, Impact of the electrical conductivity on the lithium capacity of polymer-derived silicon oxycarbide (SiOC) ceramics. Electrochim. Acta **216**, 196–202 (2016). https://doi.org/10.1016/J.ELECTACTA.2016.08.121
59. A. Klonczynski, G. Schneider, R. Riedel, R. Theissmann, Influence of boron on the microstructure of polymer derived SiCO ceramics. Adv. Eng. Mater. **6**, 64–68 (2004). https://doi.org/10.1002/adem.200300525
60. Y. Chen, F. Yang, L. An, On electric conduction of amorphous silicon carbonitride derived from a polymeric precursor. Appl. Phys. Lett. **102**, 2319021–2319024 (2013). https://doi.org/10.1063/1.4809825
61. G. Shao, W. Peng, C. Ma, W. Zhao, J. Guo, Y. Feng, et al., Enhanced electric conductivity of polymer-derived SiCN ceramics by microwave post-treatment. J. Am. Ceram. Soc. **100**, 842–847 (2017). https://doi.org/10.1111/jace.14590
62. L.-H. Hu, R. Raj, Semiconductive behavior of polymer-derived SiCN ceramics for hydrogen sensing. J. Am. Ceram. Soc. **98**, 1052–1055 (2015). https://doi.org/10.1111/jace.13520
63. C. Haluschka, C. Engel, R. Riedel, Silicon carbonitride ceramics derived from polysilazanes part II. Investigation of electrical properties. J. Eur. Ceram. Soc. **20**, 1365–1374 (2000). https://doi.org/10.1016/S0955-2219(00)00009-1
64. C. Shen, J.E. Calderon, E. Barrios, M. Soliman, A. Khater, A. Jeyaranjan, et al., Anisotropic electrical conductivity in polymer derived ceramics induced by graphene aerogels. J. Mater. Chem. C **5**, 11708–11716 (2017). https://doi.org/10.1039/C7TC03846A
65. H. Mei, Y. Xu, Y. Sun, Q. Bai, L. Cheng, Carbon nanotube buckypaper-reinforced SiCN ceramic matrix composites of superior electrical conductivity. J. Eur. Ceram. Soc. **36**, 1893–1898 (2016). https://doi.org/10.1016/J.JEURCERAMSOC.2016.02.045

66. V.S. Pradeep, D.G. Ayana, M. Graczyk-Zajac, G.D. Soraru, R. Riedel, High rate capability of SiOC ceramic aerogels with tailored porosity as anode materials for li-ion batteries. Electrochim. Acta **157**, 41–45 (2015). https://doi.org/10.1016/j.electacta.2015.01.088
67. E. Ionescu, A. Francis, R. Riedel, Dispersion assessment and studies on AC percolative conductivity in polymer-derived Si–C–N/CNT ceramic nanocomposites. J. Mater. Sci. **44**, 2055–2062 (2009). https://doi.org/10.1007/s10853-009-3304-3
68. Y. Chen, X. Yang, Y. Cao, L. An, Effect of pyrolysis temperature on the electric conductivity of polymer-derived silicoboron carbonitride. J. Eur. Ceram. Soc. **34**, 2163–2167 (2014). https://doi.org/10.1016/J.JEURCERAMSOC.2014.03.012
69. P.A. Ramakrishnan, Y.T. Wang, D. Balzar, L. An, C. Haluschka, R. Riedel, et al., Silicoboron-carbonitride ceramics: a class of high-temperature, dopable electronic materials. Appl. Phys. Lett. **78**, 3076–3078 (2001). https://doi.org/10.1063/1.1370540
70. A.M. Hermann, Y. Wang, P.A. Ramakrishnan, C. Haluschka, R. Riedel, Structure and electronic transport properties of Si-(B)-C-N ceramics. J. Am. Ceram. Soc. **84**, 2260–2264 (2001). https://doi.org/10.1111/j.1151-2916.2001.tb00999.x
71. Y. Wang, L. Zhang, W. Xu, T. Jiang, Y. Fan, D. Jiang, et al., Effect of thermal initiator concentration on the electrical behavior of polymer-derived amorphous silicon carbonitrides. J. Am. Ceram. Soc. **91**, 3971–3975 (2008). https://doi.org/10.1111/j.1551-2916.2008.02782.x
72. Y. Yu, F. Xia, Q. Huang, J. Fang, L. An, Electrical conductivity of silicon carbonitride-reduced graphene oxide composites. J. Am. Ceram. Soc. **100**, 5113–5119 (2017). https://doi.org/10.1111/jace.15025
73. B. Ma, Y. Wang, Fabrication of dense polymer-derived silicon carbonitride ceramic bulks by precursor infiltration and pyrolysis processes without losing piezoresistivity. J. Am. Ceram. Soc. **101**, 2752–2759 (2018). https://doi.org/10.1111/jace.15442
74. B. Ma, Y. Wang, K. Wang, X. Li, J. Liu, L. An, Frequency-dependent conductive behavior of polymer-derived amorphous silicon carbonitride. Acta Mater. **89**, 215–224 (2015). https://doi.org/10.1016/J.ACTAMAT.2015.02.020
75. D. Shopova-Gospodinova, Z. Burghard, T. Dufaux, M. Burghard, J. Bill, Mechanical and electrical properties of polymer-derived Si–C–N ceramics reinforced by octadecylamine – modified single-wall carbon nanotubes. Compos. Sci. Technol. **71**, 931–937 (2011). https://doi.org/10.1016/J.COMPSCITECH.2011.02.013
76. F. Ye, L. Zhang, X. Yin, Y. Zhang, L. Kong, Y. Liu, et al., Dielectric and microwave-absorption properties of SiC nanoparticle/SiBCN composite ceramics. J. Eur. Ceram. Soc. **34**, 205–215 (2014). https://doi.org/10.1016/J.JEURCERAMSOC.2013.08.005
77. F. Ye, L. Zhang, X. Yin, Y. Zhang, L. Kong, Q. Li, et al., Dielectric and EMW absorbing properties of PDCs-SiBCN annealed at different temperatures. J. Eur. Ceram. Soc. **33**, 1469–1477 (2013). https://doi.org/10.1016/J.JEURCERAMSOC.2013.01.006
78. Y. Cao, Y. Gao, R. Zhao, L. An, Coupling effect of temperature and stress on the electronic behavior of amorphous SiAlCO. J. Am. Ceram. Soc. **99**, 1881–1884 (2016). https://doi.org/10.1111/jace.14260
79. Y. Cao, X. Yang, L. An, Electric conductivity and microstructure evolution of polymer-derived SiAlCO ceramics. Ceram. Int. **42**, 4033–4038 (2016). https://doi.org/10.1016/J.CERAMINT.2015.11.073
80. G.D. Sorarù, G. Kacha, R. Campostrini, A. Ponzoni, M. Donarelli, A. Kumar, et al., The effect of B-doping on the electrical conductivity of polymer-derived Si(B)OC ceramics. J. Am. Ceram. Soc. **100**, 4611–4621 (2017). https://doi.org/10.1111/jace.14986
81. S. Trassl, M. Puchinger, E. Rössler, G. Ziegler, Electrical properties of amorphous SiCxNyHz-ceramics derived from polyvinylsilazane. J. Eur. Ceram. Soc. **23**, 781–789 (2003). https://doi.org/10.1016/S0955-2219(02)00155-3
82. N.F. Mott, Conduction in non-crystalline materials. Philos. Mag. **19**, 835–852 (1969). https://doi.org/10.1080/14786436908216338
83. X. Li, K. Wang, B. Ma, H. Hong, M. Zhang, J. Liu, et al., Effect of acrylic acid additive on electric conductivity of polymer-derived amorphous silicon carbonitride. Ceram. Int. **41**, 7971–7976 (2015). https://doi.org/10.1016/j.ceramint.2015.02.139

84. C. Haluschka, H.-J. Kleebe, R. Franke, R. Riedel, Silicon carbonitride ceramics derived from polysilazanes Part I. Investigation of compositional and structural properties. J. Eur. Ceram. Soc. **20**, 1355–1364 (2000). https://doi.org/10.1016/S0955-2219(00)00010-8
85. P.W. Anderson, Model for the electronic structure of amorphous semiconductors. Phys. Rev. Lett. **34**, 953–955 (1975). https://doi.org/10.1103/PhysRevLett.34.953
86. M.H. Cohen, Review of the theory of amorphous semiconductors. J. Non Cryst. Solids **4**, 391–409 (1970). https://doi.org/10.1016/0022-3093(70)90068-2
87. D.S. Grierson, A.V. Sumant, A.R. Konicek, T.A. Friedmann, J.P. Sullivan, R.W. Carpick, Thermal stability and rehybridization of carbon bonding in tetrahedral amorphous carbon. J. Appl. Phys. **107**, 033523 (2010). https://doi.org/10.1063/1.3284087
88. A.C. Ferrari, J. Robertson, Interpretation of Raman spectra of disordered and amorphous carbon. Phys. Rev. B **61**, 14095–14107 (2000). https://doi.org/10.1103/PhysRevB.61.14095
89. A.C. Ferrari, J. Robertson, Resonant Raman spectroscopy of disordered, amorphous, and diamondlike carbon. Phys. Rev. B **64**, 075414 (2001). https://doi.org/10.1103/PhysRevB.64.075414
90. A.B. Kousaalya, R. Kumar, S. Packirisamy, Characterization of free carbon in the as-thermolyzed Si-B-C-N ceramic from a polyorganoborosilazane precursor. J. Adv. Ceram. **2**, 325–332 (2013). https://doi.org/10.1007/s40145-013-0079-4
91. A.B. Kousaalya, R. Kumar, B.T.N. Sridhar, Thermal conductivity of precursor derived Si–B–C–N ceramic foams using *Metroxylon sagu* as sacrificial template. Ceram. Int. **41**, 1163–1170 (2015). https://doi.org/10.1016/j.ceramint.2014.09.044
92. J. Feng, Y. Xiao, Y. Jiang, J. Feng, Synthesis, structure, and properties of silicon oxycarbide aerogels derived from tetraethylortosilicate /polydimethylsiloxane. Ceram. Int. **41**, 5281–5286 (2015). https://doi.org/10.1016/J.CERAMINT.2014.11.111
93. J.L. Oteo, M.A. Mazo, C. Palencia, F. Rubio, J. Rubio, Synthesis and characterization of silicon oxycarbide derived nanocomposites obtained through ceramic processing of TEOS/PDMS preceramic materials. J. Nano Res. **14**, 27–38 (2011). https://doi.org/10.4028/www.scientific.net/JNanoR.14.27
94. M.A. Mazo, C. Palencia, A. Nistal, F. Rubio, J. Rubio, J.L. Oteo, Dense bulk silicon oxycarbide glasses obtained by spark plasma sintering. J. Eur. Ceram. Soc. **32**, 3369–3378 (2012). https://doi.org/10.1016/J.JEURCERAMSOC.2012.03.033
95. C. Godet, Physics of bandtail hopping in disordered carbons. Diamond Relat. Mater. **12**, 159–165 (2003). https://doi.org/10.1016/S0925-9635(03)00017-7
96. C. Godet, Hopping model for charge transport in amorphous carbon. Philos. Mag. B **81**, 205–222 (2001). https://doi.org/10.1080/13642810108216536
97. C. Godet, Variable range hopping revisited: the case of an exponential distribution of localized states. J. Non Cryst. Solids **299–302**, 333–338 (2002). https://doi.org/10.1016/S0022-3093(01)01008-0
98. W.D. KINGERY, M.C. McQUARRIE, Thermal conductivity: I, concepts of measurement and factors affecting thermal conductivity of ceramic materials. J. Am. Ceram. Soc. **37**, 67–72 (1954). https://doi.org/10.1111/j.1551-2916.1954.tb20100.x
99. D.T. Morelli, G.A. Slack, *High Lattice Thermal Conductivity Solids. High Thermal Conductivity Materials* (Springer-Verlag, New York, 2006), pp. 37–68. https://doi.org/10.1007/0-387-25100-6_2
100. C. Stabler, A. Reitz, P. Stein, B. Albert, R. Riedel, E. Ionescu, Thermal properties of SiOC glasses and glass ceramics at elevated temperatures. Materials **11**, 279 (2018). https://doi.org/10.3390/ma11020279
101. A. Gurlo, E. Ionescu, R. Riedel, D.R. Clarke, The thermal conductivity of polymer-derived amorphous Si-O-c compounds and nano-composites. J. Am. Ceram. Soc. **99**, 281–285 (2016). https://doi.org/10.1111/jace.13947
102. J. Yang, J. Sprengard, L. Ju, A. Hao, M. Saei, R. Liang, et al., Three-dimensional-linked carbon fiber-carbon nanotube hybrid structure for enhancing thermal conductivity of silicon carbonitride matrix composites. Carbon **108**, 38–46 (2016). https://doi.org/10.1016/J.CARBON.2016.07.002

103. L. Qiu, Y.M. Li, X.H. Zheng, J. Zhu, D.W. Tang, J.Q. Wu, et al., Thermal-conductivity studies of macro-porous polymer-derived SiOC ceramics. Int. J. Thermophys. **35**, 76–89 (2014). https://doi.org/10.1007/s10765-013-1542-8
104. O. Majoulet, F. Sandra, M.C. Bechelany, G. Bonnefont, G. Fantozzi, L. Joly-Pottuz, et al., Silicon–boron–carbon–nitrogen monoliths with high, interconnected and hierarchical porosity. J. Mater. Chem. A **1**, 10991 (2013). https://doi.org/10.1039/c3ta12119d
105. A.M. Hermann, Y.-T. Wang, P.A. Ramakrishnan, C. Haluschka, R. Riedel, D. Balzar, et al., Structure and electronic transport properties of Si-(B)-C-N ceramics. J. Am. Ceram. Soc. **84**, 2260–2264 (2004). https://doi.org/10.1111/j.1151-2916.2001.tb00999.x
106. G. Cassabois, P. Valvin, B. Gil, Hexagonal boron nitride is an indirect bandgap semiconductor. Nat. Photonics **10** (2016)
107. P. Nagels, M. Rotti, R. Gevers, Thermoelectric power due to variable-range hopping. J. Non Cryst. Solids **59–60**, 65–68 (1983). https://doi.org/10.1016/0022-3093(83)90526-4